A comprehensive study of Heisenberg-like systems with internal spin fluctuation

2003 J. Phys.: Condens. Matter 15 2783

(http://iopscience.iop.org/0953-8984/15/17/328)

INSTITUTE OF PHYSICS PUBLISHING JOURNAL OF PHYSICS: CONDENSED MATTER

J. Phys.: Condens. Matter **15** (2003) 2783–2796 PII: S0953-8984(03)58432-6

A comprehensive study of Heisenberg-like systems with internal spin fluctuation

Huai-Yu Wang[1], **Shan-Ying Wang**[1], **Chong-Yu Wang**[1], **Wen-Hui Duan**[1] **and Ke-Qiu Chen**[2,1]

[1] Department of Physics, Tsinghua University, Beijing 100084, China
[2] CCAST(World Laboratory), PO Box 8730, Beijing 100080, China

Received 1 November 2002, in final form 4 February 2003
Published 22 April 2003
Online at stacks.iop.org/JPhysCM/15/2783

Abstract

The magnetic systems described by a two-spin-per-site Heisenberg-like Hamiltonian are investigated in detail. When there are two sub-spins in one site, the magnetic behaviour becomes more complicated than usual Heisenberg systems due to the internal spin fluctuation. Spontaneous magnetization with the variation of temperature is calculated. The quantitative phase diagrams are given for ferromagnetic and antiferromagnetic states and qualitative phase diagrams are shown for mixed states. The roles played by sub-spin quantum number values, four exchange parameters and single-ion anisotropy are studied. The research gives us a comprehensive understanding of the magnetic systems with internal spin fluctuation.

1. Introduction

The Heisenberg exchange model is famous as it describes magnetic systems very well. Usually, there is one spin at each lattice site and the nearest neighbour interaction is determined by the inner product of the spins. There is no more complex structure in each lattice site. Recently, the spin fluctuation in lattice sites has been noticed. For transition metal elements, the 3d energy level splits due to the interaction of crystal fields. Often, the 3d orbitals split into two energy levels, i.e. double degenerate e_g orbitals and triple degenerate t_g orbitals under cubic and octahedral crystal fields. It is possible that spins can occupy both the split orbitals. Experimentally, a Co^{3+} ion shows such a behaviour [1]. Band structure calculations show that the electrons can indeed distribute in both e_g and t_g orbitals to form a high-spin state [2]. Although the higher-spin states in experiments are due to thermo-excitation, it is interesting to study the model that there are more than one spin in each lattice site.

Xia *et al* [3] thought that the total atom spin was composed of two spins S^d and S^t contributed by the double and triple states. Based on this consideration, they suggested a model Hamiltonian to mimic the spin fluctuation inside an atom in transition metal elements. This was an extended Heisenberg Hamiltonian in which there are two sub-spins in each lattice

site, which, hereafter, will be called a two-spin-per-site Heisenberg Hamiltonian (TSPSHH). They studied the spontaneous magnetization and susceptibility of ferromagnetism described by such a Hamiltonian by the many-body Green function method. Jiang *et al* [4] added a uniaxial anisotropy term to study its effect on the system, especially the shift of Curie point, by mean-field theory (MFT). Both of the works merely studied the ferromagnetic state. However, because of the existence of two sub-spins in one lattice site, the possible states can be very complicated.

In the usual Heisenberg Hamiltonian, the magnetic state is mainly determined by two factors: the spin quantum number S in each site and the exchange interaction J between the nearest neighbouring sites. In the case that the spin quantum number S on every site is the same, the phase diagram is simple. Below the order–disorder transition temperature, the system is either ferromagnetic when $J < 0$ or antiferromagnetic when $J > 0$. In the system described by TSPSHH, we have the following factors to be considered: the spin quantum number of the two sub-spins (S^d, S^t) in each site and the four exchange interactions between them. The possible states are determined not only by the relative orientation of neighbouring spins but also the relative orientation of the sub-spins in the one site. Recently, we [5] have found there were two remarkable features of TSPSHH due to the interactions between the spins in one site. One is that the system can show magnetism in an intermediate temperature range between 0 K and the order–disorder transition point, which can be either ferromagnetism or antiferromagnetism. The other is that a transition can occur below the order–disorder transition point. To have a clearer view of such a system, a more systematic study is needed.

Because there are two sub-spins in each site, there are six possible states. For the sake of convenience, we draw the six possible states in figure 1. States A and B are ferromagnetic and states C and D are antiferromagnetic, where B and D states may show nonmagnetism if the sub-spin quantum numbers are the same. E and F represent mixed states. Here the states mean the situations under the order–disorder transition temperature. Which state the system shows is determined by the competition of the two sub-spins and four exchange parameters. This paper is intended to thoroughly study the system described by TSPSHH to provide a comprehensive understanding of the Hamiltonian. A quantitative phase diagram is given for the ferromagnetic and antiferromagnetic cases, and a qualitative phase diagram is given for the other cases. The effect of a single ion is also discussed.

2. Hamiltonian and formula

The model assumes a simple cubic (sc) lattice. Because our discussion involves the antiferromagnetic case, the lattice is divided into two sub-lattices. Assuming that S^d and S^t are sub-spin quantum numbers in the d state and t state, respectively, in one site, the TSPSHH is

$$\begin{aligned} H = &- \sum_{(ia,jb)} (\, \boldsymbol{S}^d_{ia} \quad \boldsymbol{S}^t_{ia}\,) \cdot \begin{pmatrix} J_1 & J_3 \\ J_3 & J_2 \end{pmatrix} \begin{pmatrix} \boldsymbol{S}^d_{jb} \\ \boldsymbol{S}^t_{jb} \end{pmatrix} - \tfrac{1}{2} \sum_{ia} (\, \boldsymbol{S}^d_{ia} \quad \boldsymbol{S}^t_{ia}\,) \cdot \begin{pmatrix} 0 & J_0 \\ J_0 & 0 \end{pmatrix} \begin{pmatrix} \boldsymbol{S}^d_{ia} \\ \boldsymbol{S}^t_{ia} \end{pmatrix} \\ &- \tfrac{1}{2} \sum_{ib} (\, \boldsymbol{S}^d_{ib} \quad \boldsymbol{S}^t_{ib}\,) \cdot \begin{pmatrix} 0 & J_0 \\ J_0 & 0 \end{pmatrix} \begin{pmatrix} \boldsymbol{S}^d_{ib} \\ \boldsymbol{S}^t_{ib} \end{pmatrix} \\ &- \sum_{ia} (\, \boldsymbol{S}^d_{ia} \quad \boldsymbol{S}^t_{ia}\,) \cdot \begin{pmatrix} D_0 & D_0 \\ D_0 & D_0 \end{pmatrix} \begin{pmatrix} \boldsymbol{S}^d_{ia} \\ \boldsymbol{S}^t_{ia} \end{pmatrix} \\ &- \sum_{ib} (\, \boldsymbol{S}^d_{ib} \quad \boldsymbol{S}^t_{ib}\,) \cdot \begin{pmatrix} D_0 & D_0 \\ D_0 & D_0 \end{pmatrix} \begin{pmatrix} \boldsymbol{S}^d_{ib} \\ \boldsymbol{S}^t_{ib} \end{pmatrix}. \end{aligned} \tag{1}$$

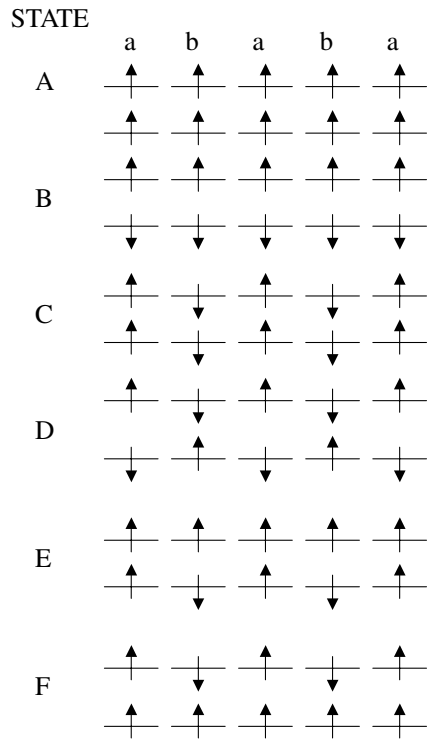

Figure 1. Possible states. In each state, the upper line means sub-spin S^d and the lower line means sub-spin S^t. The length of the arrows does not mean the dimension of the magnetization.

The first term is Heisenberg exchange between the nearest neighbouring sites. J_1 and J_2 are direct exchange and J_3 is cross exchange between neighbouring sub-spins $\boldsymbol{S}^d$ and $\boldsymbol{S}^t$, respectively. The next two terms are the intra-site exchange interaction between the two sub-spins. J_0 is on-site exchange. The last two terms represent single-ion anisotropy [4]. In equation (1), the subscripts a and b label the two sub-lattices and the summation (ia, jb) means that the summation is taken over all the nearest neighbour pairs. In this paper the sub-spin quantum numbers for the two sub-lattices are taken as the same, that is to say, $S_a^d = S_b^d = S^d$ and $S_a^t = S_b^t = S^t$. The statistical averages of the sub-spin operators are $\langle S_a^{dz}\rangle$, $\langle S_b^{dz}\rangle$, $\langle S_a^{tz}\rangle$ and $\langle S_b^{tz}\rangle$, respectively. The magnetizations of the two sub-lattices are $\langle S_a^z\rangle = \langle S_a^{dz}\rangle + \langle S_a^{tz}\rangle$ and $\langle S_b^z\rangle = \langle S_b^{dz}\rangle + \langle S_b^{tz}\rangle$. We let the exchange parameters be dimensionless as in [3–5].

The method we use is the many-body Green function theory which has long been used to treat the Heisenberg exchange model [3, 6–8]. The retarded Green functions or double-time Green functions are, according to Bogolyubov and Tyablikov [9], as follows:

$$G_{ij}(t-t') = \langle\langle A_i; B_j\rangle\rangle = -\mathrm{i}\theta(t-t')\langle A_iB_j - B_jA_i\rangle, \tag{2}$$

where the subscripts i, j label lattice sites. The Green function is Fourier time transformed and we have the equation of motion:

$$\omega\langle\langle A_i; B_j\rangle\rangle = \langle[A_i, B_j]\rangle + \langle\langle[A_i, H]; B_j\rangle\rangle. \tag{3}$$

Then the Green function is further Fourier transformed in three-dimensional real space:

$$G_{jk} = \frac{1}{N}\sum_{\boldsymbol{k}} g(\boldsymbol{k})\mathrm{e}^{\mathrm{i}\boldsymbol{k}\cdot(i-j)}. \tag{4}$$

The bold lower case letter $\boldsymbol{k}$ represents wavevectors. The integration of the wavevector $\boldsymbol{k}$ is in three dimensions. Now the Green function g is a function of wavevector $\boldsymbol{k}$ and frequency $\omega = \omega(\boldsymbol{k})$. There is a well-known spectral theorem [6, 10] to allow one to calculate the statistical average of the product of the operators:

$$\langle B_j A_i \rangle = \frac{\mathrm{i}}{2\pi N} \sum_{\boldsymbol{k}} \mathrm{e}^{\mathrm{i}\boldsymbol{k}\cdot(i-j)} \int \frac{\mathrm{d}\omega}{\mathrm{e}^{\beta\omega} - 1} [g(\boldsymbol{k}, \omega + \mathrm{i}0^+) - g(\boldsymbol{k}, \omega - \mathrm{i}0^+)]. \quad (5)$$

This formula helps us to calculate the magnetization of each sub-lattice. In considering single-ion anisotropy, Anderson–Callen's decoupling [11] is employed. Frobrich *et al* [12] showed that this decoupling was a comparatively good approximation.

In this paper, the operator A is taken as $A = S_a^{d+}, S_b^{d+}, S_a^{t+}, S_b^{t+}$. If we denote $(S_a^{d+}, S_b^{d+}, S_a^{t+}, S_b^{t+}) = (S_1^+, S_2^+, S_3^+, S_4^+)$, or simply $A = S_\alpha^+$, $\alpha = 1, 2, 3, 4$, then a set of linear equations is obtained:

$$\sum_\lambda (\omega_\lambda \delta_{\alpha\lambda} - P_{\mu\lambda}) g_{\lambda\beta} = \langle [S_\alpha^+, B_\beta] \rangle. \quad (6)$$

The elements of the matrix $\boldsymbol{P}$ are given in the appendix. To solve equations (6), one should first find the eigenvalues ω_λ and corresponding eigenvectors $U_{\lambda\nu}$ of the matrix $\boldsymbol{P}$ by solving

$$\sum_\lambda (\omega_\lambda \delta_{\mu\lambda} - P_{\mu\lambda}) U_{\lambda\nu} = 0. \quad (7)$$

Then the solution of equations (6) is expressed by

$$g_{\alpha\beta} = \sum_{\tau,\lambda} \frac{U_{\alpha\tau} U_{\tau\lambda}^{-1}}{\omega - \omega_\tau} \langle [S_\lambda^+, B_\beta] \rangle, \quad (8)$$

where U^{-1} is the inverse matrix of U. Employing the spectral theorem equation (5), we have

$$\langle B_\beta S_\alpha^+ \rangle = \sum_{\tau,\lambda} \frac{U_{\alpha\tau} U_{\tau\lambda}^{-1}}{\mathrm{e}^{\beta\omega_\tau} - 1} \langle [S_\lambda^+, B_\beta] \rangle. \quad (9)$$

If we choose $B_\beta = (S_\beta^z)^n S_\beta^-$ and define

$$R_\alpha = \frac{1}{N} \sum_{\boldsymbol{k}} \sum_\tau \frac{U_{\alpha\tau} U_{\tau\alpha}^{-1}}{\mathrm{e}^{\beta\omega_\tau} - 1}, \qquad \alpha = 1, 2, 3, 4, \quad (10)$$

the statistical averages of the spin operators $\langle S_\alpha^z \rangle$ can be evaluated by the following formula [13]:

$$\langle S_\alpha^z \rangle = \frac{(S_\alpha - R_\alpha)(1 + R_\alpha)^{2S_\alpha+1} + (1 + S_\alpha + R_\alpha) R_\alpha^{2S_\alpha+1}}{(1 + R_\alpha)^{2S_\alpha+1} - R_\alpha^{2S_\alpha+1}}, \qquad \alpha = 1, 2, 3, 4, \quad (11)$$

where we denote spin averages $(\langle S_a^{dz} \rangle, \langle S_b^{dz} \rangle, \langle S_a^{tz} \rangle, \langle S_b^{tz} \rangle) = (\langle S_1^z \rangle, \langle S_2^z \rangle, \langle S_3^z \rangle, \langle S_4^z \rangle)$ and the sub-spin quantum numbers $(S_a^d, S_b^d, S_a^t, S_b^t) = (S_1, S_2, S_3, S_4)$.

These equations are self-consistent equations. In calculation, an initial state, composed by a set of magnetizations $\{\langle S_\alpha^z \rangle\}$, are put into the equations to produce the resultant magnetization. The iteration goes on until convergence is reached. If the calculation does not converge or the resulting statistical average is larger than the spin quantum number, e.g. $|\langle S_\alpha^z \rangle| > S_\alpha$, we say that the system is frustrated. That means that, under some parameters, there is no stable state.

Apparently, when $\langle S_a^{dz} \rangle = \langle S_b^{dz} \rangle$ and $\langle S_a^{tz} \rangle = \langle S_b^{tz} \rangle$, the system is ferromagnetic and goes back to the case studied by Xia *et al* [3]. We first retrieve all of Xia *et al*'s [3] results by the above formula.

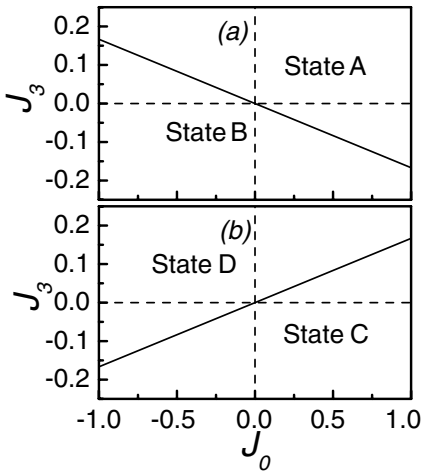

Figure 2. Phase diagrams involving states A, B, C and D with parameters (a) $J_1 > 0$, $J_2 > 0$ and (b) $J_1 < 0$, $J_2 < 0$. The associated parameters are listed in table 1. The broken lines are only to show that the full line is through the origin.

3. Results and discussion

3.1. The states without single-ion anisotropy

First, let us discuss the case of $D_0 = 0$.

3.1.1. Ferromagnetic states. If $J_1 > 0$, $J_2 > 0$ and $J_3 = J_0 = 0$, then $\boldsymbol{S}_a^d$ is parallel to $\boldsymbol{S}_b^d$ and $\boldsymbol{S}_a^t$ parallel to $\boldsymbol{S}_b^t$. The system can be either in state A or B. It will be in state A if both J_3 and J_0 are positive, and will be in state B if both J_3 and J_0 are negative. Now suppose that the signs of J_3 and J_0 are opposite: the state will then be determined by the difference in strengths of these two parameters. The phase diagram is calculated for parameters J_3 and J_0, as in figure 2(a). There is a line separating the two states A and B. Above the line the state is A, and the other side is state B. The boundary line in figure 2(a) can be expressed by

$$J_3 = -\tfrac{1}{6}J_0. \tag{12}$$

The parameters associated with the phase diagram are listed in table 1. It is seen that, if we change the sub-spin values and interactions J_1 and J_2, the phase diagram remains unchanged. The boundary line is uniquely determined by the competition between J_3 and J_0, independent of other factors.

Usually both sub-spins have identical Curie points due to the cross and on-site exchanges, i.e. the state A with $J_3 = 0$ and $J_0 = 0.6$, as shown by the thinner lines in figure 3. However, for the states very much closer to the boundary line, the Curie points for the two sub-spins are not the same if either direct exchanges or sub-spin values of them are different. When we take the parameters as $J_3 = -0.99$ and $J_0 = 0.6$, which is a state A close to the boundary line in figure 2(a), the results are depicted in figure 3 as thicker curves. If the sub-spin values are the same, $S^d = S^t$, but their direct exchange interactions are different, say $J_1 > J_2$, the magnetization of the sub-spin with less direct exchange becomes zero rapidly, see figure 3(a). If the direct exchange interactions are the same, $J_1 = J_2$, but the sub-spin values are different, say $S^d > S^t$, the magnetization of the smaller sub-spin has a lower Curie point, as shown in

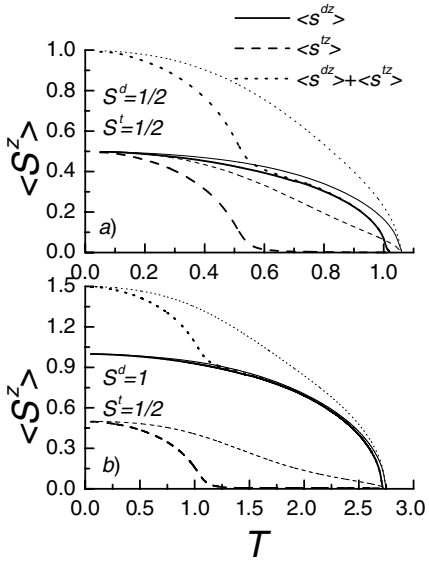

Figure 3. Spin averages versus temperature. The state is A so that the two sub-lattices are identical. $J_1 = 1$, $J_0 = 0.6$. (a) $J_2 = 0.5$. In this case, the two sub-spin quantum numbers are same, but the direct exchange between S^t is less than that of S^d, $J_1 > J_2$. (b) $J_2 = 1$. In this case, the two direct exchanges are the same, $J_1 = J_2$, but $S^{dz} > S^{tz}$. Thin curves are for $J_3 = 0$, while thick curves are for $J_3 = -0.99$, a state very much closer to the boundary line in figure 2(a).

figure 3(b). In both cases, if the parameters, say J_3, are varied to leave the boundary curve, the lower Curie point will rise and the thicker curves in figure 3 will tend towards the thinner lines.

The fact that, at the boundary line, the two sub-spins have their own Curie points reveals that their behaviour is determined by their own direct exchange, independent of other factors, that is to say, the cross and on-site exchanges are negligible. Hence along the boundary line J_3 and J_0 counteract and the synthesized effect is nearly zero. Because the effect of J_1 and J_2 (both being positive) is to make neighbouring spins parallel, J_3 and J_0 should have opposite signs to counteract each other. So the slope of the boundary line in figure 2(a) is negative. At the line, the ratio $|J_0/J_3|$ is 6. That means that one share of on-site exchange can counteract six shares of cross exchange interactions. Compared to the cross exchange, the on-site exchange plays a more important role. Since along the boundary line, the effect of cross and on-site interactions are negligible, the order–disorder transition temperature reaches its lowest value, as shown in figures 4 and 5.

Figure 4 shows the curves of T_c versus J_3 for parameters $J_1 = 1$, $J_2 = 0.5$ and $J_0 = 0.2$. It is seen that, under the same exchange strengths, larger sub-spin quantum numbers lead to larger T_c. On the other hand, under the same sub-spin quantum numbers, larger exchange strengths lead to larger T_c. The appearance of intersecting points P_1 and P_2 can be analysed as follows. When $J_3 = 0$ and $J_0 = 0$, the critical point of the system with spins $(1/2, 3/2)$ is smaller than the system with spins $(1, 1/2)$. This is because the critical point is mainly subject to the larger direct coupling when the cross exchange is absent. With the same direct coupling, the larger spin value system should have a higher critical point. When $J_{P1} < J_3 < J_{P2}$, the cross exchange is not strong enough to change this situation. As J_3 is large enough, the cross exchange becomes dominant and the critical point is subject to the larger total spin. The critical point is determined by the competition of the exchange J_3 and J_0 when the spin values and the

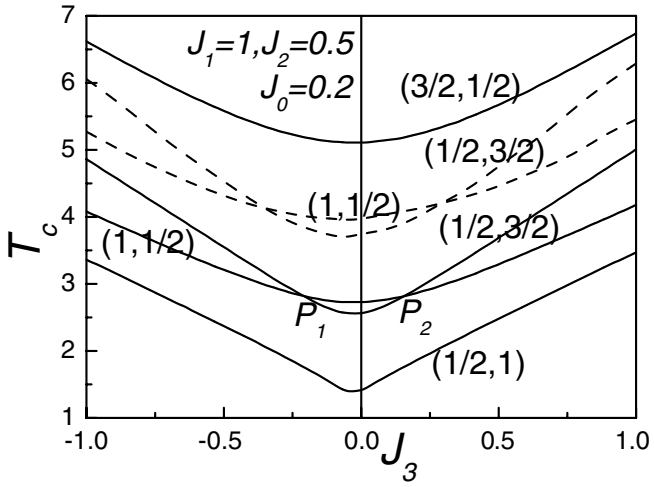

Figure 4. Critical point T_c versus cross exchange interaction J_3. The other parameters are: $J_1 = 1$, $J_2 = 0.5$ and $J_0 = 0.2$. The figures in parentheses are the two sub-spin quantum numbers. Note that the lowest T_c values are at the positions where J_3 is about -0.033. As a comparison, we also depict the results of MFT [4] as broken curves.

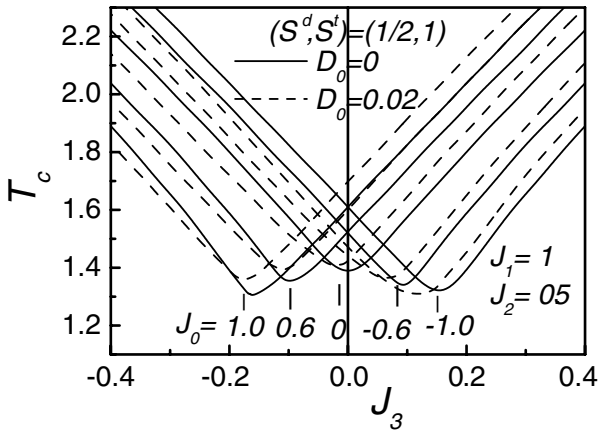

Figure 5. Critical point T_c versus cross exchange interaction J_3 to see the positions of the valleys depending on the J_0 value and the effect of single-ion anisotropy. The other parameters are: $J_1 = 1$, $J_2 = 0.5$. As $D_0 = 0$, the valleys are at the positions described by $J_0 = -\frac{1}{6}J_3$, i.e. the boundary line in figure 2(a). As $D_0 = 0.02$, the valleys move leftward slightly.

coupling parameters J_1 and J_2 are fixed. We also copy the results by MFT [4]. It is obvious that the MFT overestimates the Curie point.

We call the position where the T_c has its lowest value as J_{3m}. Note that, in figure 4, J_{3m} is not zero, but is at the position $J_{3m} = -0.033$. This is because, $J_0 = 0.2$, not zero. If $J_0 = 0$, the valley is at the position $J_3 = 0$, see figure 5. The full curves in figure 5 show the $T_c - J_3$ curves for five J_0 values. The valleys of T_c for $J_0 = \pm 1, \pm 0.6, 0$ are at the positions $J_{3m} = \mp 0.166, \mp 0.1, 0$, which are along the boundary line of figure 2(a).

Note that in either state A or B, the system is ferromagnetic. In [4], the cases with parameters $J_1 = 1$, $J_2 = 0.5$ and $J_0 = 0.2$ and $J_3 < 0$, which are state B here, were thought to

Table 1. Parameters that the phase diagrams in figure 2 have.

(S^d, S^t)	$J_1 = 1, J_2 = 1$	$J_1 = 1, J_2 = 0.5$	$J_1 = -1, J_2 = -1$	$J_1 = -1, J_2 = -0.5$
(1/2, 1/2)	Figure 2(a)	Figure 2(a)	Figure 2(b)	Figure 2(b)
(1, 1/2)	Figure 2(a)	Figure 2(a)	Figure 2(b)	Figure 2(b)
(1, 1)	Figure 2(a)	Figure 2(a)	Figure 2(b)	Figure 2(b)
(3/2, 1)	Figure 2(a)	Figure 2(a)	Figure 2(b)	Figure 2(b)

be antiferromagnetic. In state B, the spin orientation of neighbouring sites is the same. On the other hand, for antiferromagnetic cases, the spins of neighbouring sites should be antiparallel as state C or D, so that the lattice must be treated by dividing it into two sub-lattices. The condition that the system be antiferromagnetic is that at least one of the direct exchanges must be negative.

For the case of state B when $S^d = S^t$, $J_1 = J_2$, the total magnetization is zero and the system will not exhibit magnetism at any temperature. However, if $S^d = S^t$ but $J_1 \neq J_2$, the system will still be ferromagnetic. In figure 2 of [5], we showed such a case. At zero temperature, the two sub-spins are antiparallel to each other and the system will not exhibit magnetism. As temperature increases, the sub-spin with larger direct exchange has larger magnetization. Therefore, the net magnetization is not zero and the system manifests ferromagnetism until the Curie point.

3.1.2. Antiferromagnetic states. If $J_1 < 0$, $J_2 < 0$ and $J_3 = J_0 = 0$, then S_a^d is antiparallel to S_b^d and S_a^t is antiparallel to S_b^t. The system can be in either state C or D. As the cross exchange and on-site exchange become nonzero, the competition of the two parameters determines the state of the system. The phase diagram is calculated as in figure 2(b). There is also a line separating the states C and D. Above the line is state D, and the other side is state C. The boundary line in figure 2(b) can be expressed by

$$J_3 = \tfrac{1}{6} J_0. \tag{13}$$

Because the effect of J_1 and J_2 (both being negative) now is to make neighbouring spins antiparallel, J_3 and J_0 should have the same sign to counteract each other, so that the slope of the boundary line is positive. Still, six shares of cross exchange can compete to one share of on-site exchange. The parameters associated with the phase diagram are listed in table 1. Again it is seen that, if we change sub-spin values and interactions J_1 and J_2, the phase diagram is unchanged. The boundary line is uniquely determined by the competition between J_3 and J_0, independent of other factors. Figures 2(a) and (b) are so similar that one can change the former to be the latter by the following simple manipulations. The slope of the boundary line is changed from negative to positive, and state A is replaced by state D and state B by state C. Subsequently, the analysis of antiferromagnetic states is similar to that of the ferromagnetic states. Having analysed ferromagnetic states in detail, the understanding of antiferromagnetic states is relatively simple. We merely state the conclusions.

Along the boundary line in figure 2(b), the cross and on-site exchanges counteract each other. Close to the line, the two sub-spins have their own Curie point as if they are independent of each other. The sub-spin with smaller spin quantum number or weaker direct exchange will have a lower Curie point. However, if the parameters J_3 and J_0 are chosen such that they are far away from the boundary line in figure 2(b), the two sub-spins will possess one common Curie point. This discussion is similar to that for figure 3.

Figure 6 shows the curves of T_c versus J_3 for parameters $J_1 = 1$, $J_2 = 0.5$ and $J_0 = 0.2$. Under the same exchange strengths, larger sub-spin quantum numbers lead to larger T_c.

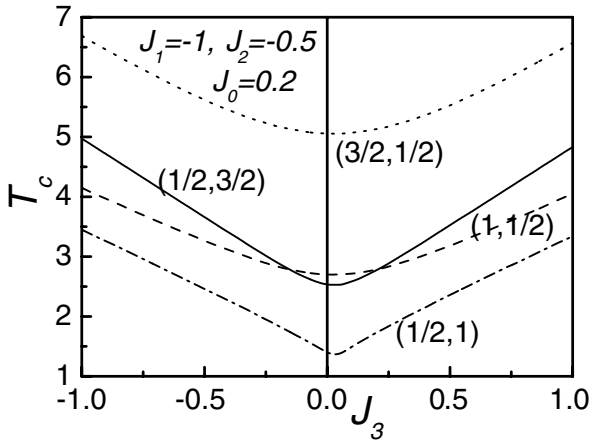

Figure 6. Critical point T_c versus cross exchange interaction J_3. The other parameters are: $J_1 = -1$, $J_2 = -0.5$ and $J_0 = 0.2$. The figures in parentheses are the two sub-spin quantum numbers. Note that the lowest T_c values are at the positions where J_3 is about 0.033.

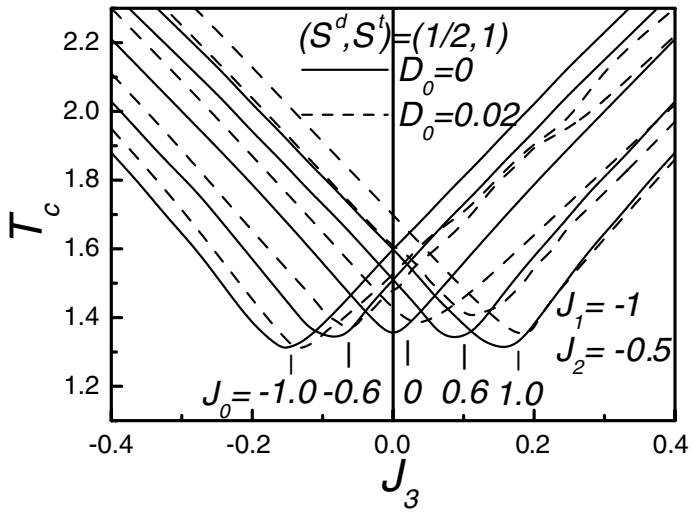

Figure 7. Critical point T_c versus cross exchange interaction J_3 to see the positions of valleys versus J_0 value and the effect of single-ion anisotropy. The other parameters are: $J_1 = -1$, $J_2 = -0.5$. As $D_0 = 0$, the valleys are at the positions described by $J_0 = \frac{1}{6}J_3$, i.e. the boundary line in figure 2(b). As $D_0 = 0.02$, the valleys move rightwards slightly.

On the other hand, under the same sub-spin quantum numbers, larger exchange strengths lead to larger T_c. The feature is the same as in figure 4. Now the lowest T_c value is at the position $J_{3m} = 0.033$. This is because the slope of the boundary line in figure 2(b) is positive. If $J_0 = 0$, the valley is at the position $J_3 = 0$, see figure 7. The full curves in figure 7 show the $T_c - J_3$ curves for five J_0 values. The valleys of T_c for $J_0 = \pm 1, \pm 0.6, 0$ are at the positions $J_3 = \pm 0.166, \pm 0.1, 0$, respectively, which are along the boundary line in figure 2(b).

For the case of state D when $S^d = S^t$ and $J_1 = J_2$, the total magnetization is zero and the system will not exhibit magnetism at any temperature. However, if $S^d = S^t$ but $J_1 \neq J_2$,

the system will still be antiferromagnetic. As has been shown in figure 3 of [5], there can occur a case that the system exhibits antiferromagnetism in the intermediate range between zero temperature and the Curie point.

3.1.3. Mixed states. The states E and F are substantially the same. For convenience of discussion, we still distinguish them separately. If $J_1 > 0$, $J_2 < 0$ and $J_3 = J_0 = 0$, then S_a^d is parallel to S_b^d and S_a^t is antiparallel to S_b^t. The system is of state E. When cross exchange and on-site exchange become nonzero, the cases become complicated. In table 2, we post the calculated states, depending on the parameters for the sub-spins $(S^d, S^t) = (1, 1/2)$.

In table 2, E–A(B) means that at low temperature near to zero the state is E. At some temperature the system transits to state A(B). The state A(B) then lasts until the Curie point. Figures 8 and 9 show two examples. We call this transition the intermediate transition because it occurs in the intermediate temperature range between zero and the order–disorder transition. We have given a simple physical explanation of the occurrence of the intermediate transition by means of the concept of molecular field (MF) [5].

N–A(B) in table 2 means that, at low temperature near to zero, there is no solution. Here, because the effect of the four exchange parameters contrast each other, the system does not have a stable state. When temperature increases, the thermal motion is strong enough. Correspondingly, the effect of exchanges seems 'weaker' and the system can hold a stable state. Here we see that the 'strength' of thermal motion plays a role to overcome the frustration of the system.

Based on table 2, we depict the qualitative phase diagram in figure 10(a). Around the line $J_3 = 0$, the state is E–B when $J_0 < 0$ and is E–A when $J_0 > 0$. The full boundary line has the same slope, $-1/6$, as in figure 2(a). Above the dotted line the state is A and below the chain curve it is state B. The positions of these two boundary lines depend on direct exchanges, but the slopes of them are believed to be the same as the full line. From table 2, when the strengths of the two direct exchange J_1 and J_2 are closer, the broken line in figure 10(a) will move upwards and the chain curve will move downwards. That is to say, the areas of N–A and N–B will extend. Since J_1 and J_2 have different signs, any pair of on-site and cross exchanges lead to the opposite effect. The closer the strengths of the two direct exchanges, the easier for the system to be frustrated at low temperature, as illustrated by table 2. If the sub-spins are varied, the phase diagram remains qualitatively unchanged.

If $J_1 < 0$, $J_2 > 0$ and $J_3 = J_0 = 0$, then S_a^d is antiparallel to S_b^d and S_a^t is parallel to S_b^t. The system is of state F. When cross exchange and on-site exchange become nonzero, the qualitative phase diagram is figure 10(b). In order to get the phase diagram, one only needs to change the slope of the boundary lines in figure 10(a) from $-1/6$ to $1/6$ and replace the letters A, B and E by D, C and F, respectively. The procedure is almost the same as that from figures 2(a)–(b). The discussion of F-related states is similar to the above E-related states.

Comparing figure 8 with figure 9, both have the same exchange strengths, but the former has a larger sub-spin S^d and its transition temperature $T_{\mathrm{E-B}}$ is higher than $T_{\mathrm{F-D}}$ of the latter. It shows that a smaller sub-spin is more easily affected by thermal motion. Larger sub-spins result in a higher order–disorder transition, but do not necessarily lead to a higher intermediate transition point. In figures 8(a) and 9(a), the transition points are 1.43 and 1.61, respectively.

In figure 9, the total magnetization of sub-lattice b, $\langle S_b^z \rangle = \langle S_b^{dz} \rangle + \langle S_b^{tz} \rangle$ (short broken curve), is positive near zero temperature and flips under the transition point $T_{\mathrm{F-D}}$. This flip does not cause a F–D transition. Only the flip of $\langle S_b^t \rangle$ (broken line) causes the F–D transition. The flip of $\langle S_b^z \rangle$ is due to the competition of exchange parameters. If we choose $J_2 = 0.5$ and $J_0 = -0.5$, while keeping the other parameters in figure 9 unchanged, the $\langle S_b^z \rangle$ will be always negative under the order–disorder transition temperature and will not show a flip.

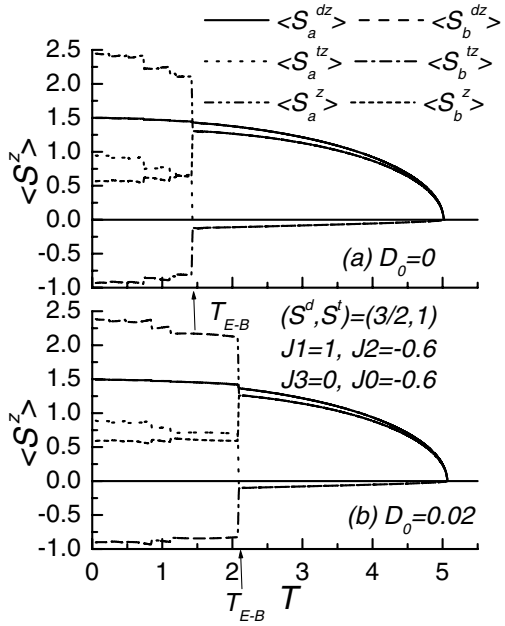

Figure 8. Spin averages versus temperature. (a) $D_0 = 0$, $T_{\mathrm{E–B}} = 1.43$, $T_c = 5.02$; (b) $D_0 = 0.02$, $T_{\mathrm{E–B}} = 2.08$, $T_c = 5.07$. At E–B transformation temperature, $T_{\mathrm{E–B}}$, the magnetization has a jump, indicating a first-order transformation. The effect of single-ion anisotropy is to increase $T_{\mathrm{E–B}}$ and the order–disorder transition point.

Table 2. States of sub-spin quantum numbers $(S^d, S^t) = (1, 1/2)$ under some exchange parameters.

$J_0 =$	−0.9	−0.6	−0.3	0	0.3	0.6	0.9
J_3				$J_1 = 1$, $J_2 = -0.5$			
0.9	N–A	A	A	A	A	A	A
0.6	N–A	N–A	A	A	A	A	A
0.3	N–A	N–A	N–A	N–A	N–A	N–A	N–A
0	E–B	E–B	E–B	E	E–A	E–A	E–A
−0.3	B	N–B	N–B	N–B	N–B	N–B	N–B
−0.6	B	B	B	B	N–B	N–B	N–B
−0.9	B	B	B	B	B	B	B
J_3				$J_1 = 1$, $J_2 = -1$			
0.9	N–A	N–A	N–A	N–A	A	A	A
0.6	N–A	N–A	N–A	N–A	N–A	N–A	A
0.3	N–A	N–A	N–A	N–A	N–A	N–A	N–A
0	N–B	E–B	E–B	E	E–A	E–A	E–A
−0.3	N–B	N–B	N–B	N–B	N–B	N–B	N–B
−0.6	B	N–B	N–B	N–B	N–B	N–B	N–B
−0.9	B	B	B	N–B	N–B	N–B	N–B

3.2. The effect of single-ion anisotropy

In [4], the anisotropic parameter D_0 was chosen as the same magnitude order of exchange parameters J. However, usually the single-ion anisotropy strength is believed to be two orders

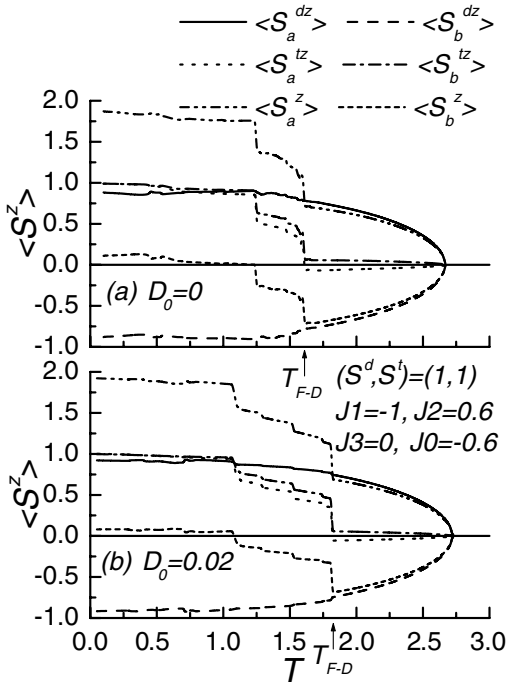

Figure 9. Spin averages versus temperature to show F–D transformation. (a) $D_0 = 0$, $T_{\mathrm{E-D}} = 1.61$, $T_c = 2.67$; (b) $D_0 = 0.02$, $T_{\mathrm{F-D}} = 1.82$, $T_c = 2.73$. At F–D transformation temperature, $T_{\mathrm{F-D}}$, the magnetization has a jump, indicating a first-order transformation. The effect of single-ion anisotropy is to increase $T_{\mathrm{F-D}}$ and the order–disorder transition point.

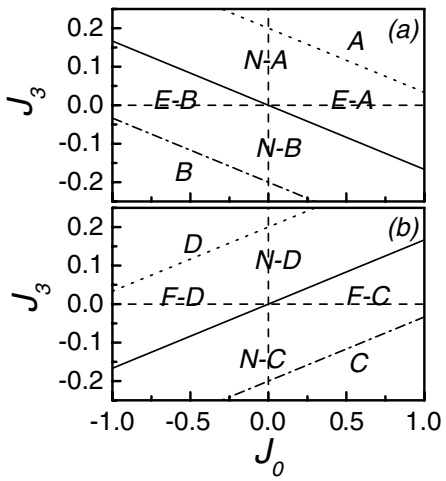

Figure 10. Qualitative phase diagrams when the parameters are (a) $J_1 > 0$ and $J_2 < 0$ and (b) $J_1 < 0$ and $J_2 > 0$. The broken lines are only to show that the full line is through the origin.

of magnitude less than the direct exchange interaction [12, 15, 16]. In this paper, we take $D_0 = 0.02$. In figure 5, it is observed that the valleys of the curves T_c versus J_3 shift leftwards

slightly due to the anisotropy. The shift can be explained qualitatively as follows. When $J_3 > J_{3m}$, the state is A, see figure 2(a). The sub-spins are parallel. The single-ion anisotropy strengthens this orientation, which leads to a stronger ability to overcome thermal movement. As a result, the Curie point rises. When $J_3 < J_{3m}$, the state is B. The two sub-spins in one site are antiparallel to each other. A single-ion anisotropy means a stronger force, making them antiparallel and, as a result, the total spin average goes to zero with temperature more quickly and T_c decreases. Therefore, the left branch of the valley in the curves descends and the right branch rises so that the valley moves leftwards.

The discussion of the single-ion effect in figure 7 is similar to that in figure 5. When $J_3 < J_{3m}$, the state is C with parallel intra-site sub-spins, and when $J_3 > J_{3m}$, the state is D with antiparallel intra-site sub-spins. The effect of single-ion anisotropy is to increase T_c of the former and to decrease T_c for the latter case, so that the valleys of the curves T_c versus J_3 shift rightwards slightly.

The single-ion anisotropy slightly lifts the order–disorder transition temperature, see figures 8 and 9 as examples. In figure 8(a), the order–disorder transition temperature is 5.02 as $D_0 = 0$. It becomes 5.07 as $D_0 = 0.02$, see figure 8(b). In figure 9, the order–disorder transition temperature is 2.67 as $D_0 = 0$ and becomes 2.73 as $D_0 = 0.02$.

The anisotropy also increases the E(F)–X(A, B, C, D) transition temperature, as can be seen from figures 8 and 9. In figure 8, the E–B transition point $T_{\mathrm{E-B}}$ is increased from 1.43 to 2.08 due to single-ion anisotropy. In figure 9, the F–D transformation point $T_{\mathrm{F-D}}$ is increased from 1.61 to 1.82. Calculations show that the larger the sub-spins, the more the increase of $T_{\mathrm{E(F)-X}}$.

By the concept of MF [5], the sub-spin S_b^t, as J_3 for instance, is subjected to two MF: on-site MF (OSMF) $J_0\langle S_b^{tz}\rangle$ and nearest neighbour MF (NNMF) $6J_2\langle S_b^{tz}\rangle$. At zero temperature, the NNMF prevails. With the increase of temperature, $\langle S_b^{tz}\rangle$ drops more quickly because $|J_2| < J_1$. At temperature $T_{\mathrm{E(F)-X}}$, transition occurs. Now the existence of single-ion anisotropy strengthens both MFs. The NNMF will last to a higher temperature before being overwhelmed by the OSMF. Thus the intermediate transition temperature $T_{\mathrm{E(F)-X}}$ rises.

4. Summary

The possible magnetic states of TSPSHH are investigated in detail by the many-body Green function method. The magnetic state is determined by the competition of sub-spin quantum numbers and four exchange parameters. Generally speaking, larger spin values and stronger exchanges lead to higher order–disorder transitions. The introduction of single-ion anisotropy increases the order–disorder transition point and intermediate transition point. Here the effect of internal spin fluctuation is obvious as it results in the intermediate transition. The quantitative phase diagrams are given for ferromagnetic and antiferromagnetic states and qualitative phase diagrams are shown for mixed states. The research gives us a comprehensive understanding of the magnetic systems with internal spin fluctuation. Although we only discuss the case for $(S_a^d, S_a^t) = (S_b^d, S_b^t)$, the case for $(S_a^d, S_a^t) \neq (S_b^d, S_b^t)$ can be studied in the same way.

Acknowledgment

This work was supported by the National Key Program of Basic Project (grant no G2000067108) of China.

Appendix

The elements of the matrix $\boldsymbol{P}$ in equation (6) are

$$
\begin{aligned}
a_{11} &= z(J_1\langle S_2^{dz}\rangle + J_3\langle S_2^{tz}\rangle) + D(\varphi_{s1}\langle S_1^{dz}\rangle + 2\langle S_1^{tz}\rangle) + J_0\langle S_1^{tz}\rangle,\\
a_{12} &= -J_1\langle S_1^{dz}\rangle\gamma_{\boldsymbol{k}}, \qquad a_{13} = -J_0\langle S_1^{dz}\rangle, \qquad a_{14} = -J_3\langle S_1^{dz}\rangle\gamma_{\boldsymbol{k}},\\
a_{21} &= -J_1\langle S_2^{dz}\rangle\gamma_{\boldsymbol{k}},\\
a_{22} &= z(J_1\langle S_1^{dz}\rangle + J_3\langle S_1^{tz}\rangle) + D(\varphi_{s2}\langle S_2^{dz}\rangle + 2\langle S_2^{tz}\rangle) + J_0\langle S_2^{tz}\rangle,\\
a_{23} &= -J_3\langle S_2^{dz}\rangle\gamma_{\boldsymbol{k}}, \qquad a_{24} = -J_0\langle S_2^{dz}\rangle,\\
a_{31} &= -J_0\langle S_1^{tz}\rangle, \qquad a_{32} = -J_3\langle S_1^{tz}\rangle\gamma_{\boldsymbol{k}},\\
a_{33} &= z(J_2\langle S_2^{tz}\rangle + J_3\langle S_2^{dz}\rangle) + D(\varphi_{t1}\langle S_1^{tz}\rangle + 2\langle S_1^{td}\rangle) + J_0\langle S_1^{dz}\rangle,\\
a_{34} &= -J_2\langle S_1^{tz}\rangle\gamma_{\boldsymbol{k}},\\
a_{41} &= -J_3\langle S_2^{tz}\rangle\gamma_{\boldsymbol{k}}, \qquad a_{42} = -J_0\langle S_2^{tz}\rangle, \qquad a_{43} = -J_2\langle S_2^{tz}\rangle\gamma_{\boldsymbol{k}},\\
a_{44} &= z(J_2\langle S_1^{tz}\rangle + J_3\langle S_1^{dz}\rangle) + D(\varphi_{t2}\langle S_2^{tz}\rangle + 2\langle S_2^{tz}\rangle) + J_0\langle S_2^{dz}\rangle.
\end{aligned}
$$

Here z is the nearest neighbour number of one site and $\gamma_{\boldsymbol{k}} = \sum \mathrm{e}^{\mathrm{i}\boldsymbol{k}\cdot\boldsymbol{\delta}}$, where δ means the position vector of the nearest neighbours.

References

[1] Zobel C, Kriener M, Bruns D, Baier J, Gruninger M, Lorentz T, Reutler P and Revcolevschi A 2002 *Phys. Rev.* B **66** 020402
Kobayashi Y, Fujiwara N, Murata S, Asai K and Yasuoka H 2000 *Phys. Rev.* B **62** 410
Moritomo Y, Akimoto T, Takeo M, Machida A, Nishibori E, Takata M, Sakata M, Ohoyama K and Nakamura A 2000 *Phys. Rev.* B **61** R13325
Roy S, Khan M, Guo Y Q, Craig J and Ali N 2002 *Phys. Rev.* B **65** 064437
Vogt T, Woodward P M, Karen P, Hunter B A, Henning P and Moodenbaugh A R 2000 *Phys. Rev. Lett.* **84** 2969
[2] Korotin M A, Ezhov S Yu, Solovyev I V, Anisimov V I, Khomskii D I and Sawatzky D A 1996 *Phys. Rev.* B **54** 5309
Abbate M, Potze R, Sawatzhy G A and Fujimori A 1994 *Phys. Rev.* B **49** 7210
Foerster D, Hayn R, Pruschke T, Zolfl M and Rosner H 2001 *Phys. Rev.* B **64** 075104
Wu H 2001 *Phys. Rev.* B **64** 092413
Wang J, Zhang W and Xing D Y 2001 *Phys. Rev.* B **64** 064418
[3] Xia K, Zhang W, Lu M and Zhai H 1997 *J. Phys.: Condens. Matter* **9** 5643
[4] Jiang Q, Jiang X F and Li Z 1999 *J. Magn. Magn. Mater.* **195** 501
[5] Wang H Y, Chen K Q and Wang E G 2002 *Phys. Rev.* B **66** 092405
[6] Tyablikov S V 1967 *Methods in the Quantum Theory of Magnetism* (New York: Plenum)
[7] Tahir-Kheli R A and Ter Haar D 1962 *Phys. Rev.* **127** 88
Tahir-Kheli R A and Ter Haar D 1962 *Phys. Rev.* **127** 95
[8] Callen H B 1963 *Phys. Rev.* **130** 890
[9] Bogolyubov N N and Tyablikov S V 1959 *Sov. Phys.–Dokl.* **4** 589
[10] Wang H Y 1998 *The Green Function Method in Physics* (Hong Kong: Science, Education and Culture Press) (in Chinese)
[11] Anderson F B and Callen H B 1964 *Phys. Rev.* A **136** 1068
[12] Frobrich P, Jensen P J and Kuntz P J 2000 *Eur. Phys. J.* B **13** 477
Frobrich P, Jensen P J, Kuntz P J and Ecker A 2000 *Eur. Phys. J.* B **18** 579
[13] Guo W, Shi L P and Lin D L 2000 *Phys. Rev.* B **62** 14259
[14] Moran T J, Nogues J, Lederman D and Schuller Ivan K 1998 *Appl. Phys. Lett* **72** 617
Jungblut R, Coehoom R, Johnson M T, Stegge Jaan De and Reinders A 1994 *J. Appl. Phys.* **75** 6659
Ijiri Y, Borchers J A, Erwin R W, Lee S H, Zaag P J van deer and Wolf R M 1998 *Phys. Rev. Lett.* **80** 608
[15] Moschel A and Usadel K D 1994 *Phys. Rev.* B **49** 12868
Moschel A and Usadel K D 1995 *Phys. Rev.* B **51** 16111
Hucht A and Usadel D K 1997 *Phys. Rev.* B **55** 12309
[16] Wang H Y, Zhou Y S, Lin D L and Wang C Y 2002 *Chin. Phys* **11** 167